Direct Observation of Vortex Shells and Magic Numbers in Mesoscopic Superconducting Disks

I. V. Grigorieva,[1,*] W. Escoffier,[1] J. Richardson,[1] L. Y. Vinnikov,[1,2] S. Dubonos,[2] and V. Oboznov[2]

[1]*School of Physics and Astronomy, University of Manchester, Oxford Road, Manchester M13 9PL, United Kingdom*

[2]*Institute of Solid State Physics, Russian Academy of Sciences, Chernogolovka 142432, Russia*

(Received 11 July 2005; published 23 February 2006)

We have studied vortex configurations in mesoscopic superconducting disks using the Bitter decoration technique. For a broad range of vorticities L the circular geometry is found to lead to the formation of concentric shells of vortices. From images obtained on disks of different sizes in a range of magnetic fields we traced the evolution of vortex states and identified stable and metastable configurations of interacting vortices. Furthermore, the analysis of shell filling with increasing L allowed us to identify magic numbers corresponding to the appearance of consecutive new shells.

DOI: 10.1103/PhysRevLett.96.077005 PACS numbers: 74.25.Qt, 74.25.Ha, 74.78.Na

The properties of a type-II superconductor change dramatically as it becomes mesoscopic [1–10], i.e., can accommodate only a small number of vortices. In a magnetic field H, such a superconductor resides in one of a series of discrete states characterized by the vorticity L. Vortex states in mesoscopic superconductors have attracted a lot of interest, especially since the prediction of two different kinds of vortex states—the multivortex state with L singly quantized vortices [1–4] and a giant-vortex state for the same L [5,6]. This has prompted many studies that continue to bring surprises such as symmetry-induced antivortices [7], the paramagnetic Meissner effect [8], giant [9] and fractional-flux [10] vortices, vortices trapped in blind holes [11], etc. On the other hand, vortices in small superconductors can be viewed as a representative of finite systems of interacting particles (e.g., ''artificial atoms'' [12], vortices in superfluids [13,14], etc.). Particle arrangements in such systems strongly depend on the number of particles involved, which is governed by rich and subtle physics arising due to the competition between particle interaction and confinement [2–4,12,13]. The number of particles required to fill consecutive shells that appear in circular geometries (so-called ''magic numbers'') has always attracted special interest ([12,13], and references therein).

In the case of superconductors, numerical studies focused either on small disks, where stable and metastable configurations were found for $L \leq 11$ [2–4], or relatively large ($L > 100$) disks, where formation of the triangular lattice becomes a dominant feature [15]. None of the predicted configurations has so far been observed directly, whereas states for intermediate vorticities $10 < L < 100$ remain largely unknown even in theory. Additional kinks in magnetization and tunneling curves observed in Al disks [9,16] indicated changes in vortex configurations but could not prove what those configurations were. A recent attempt to visualize vortices using scanning SQUID [17] was limited to a maximum of 3 vortices in large (30–50 μm) square and triangular samples. In this Letter, we report the first direct observation of vortex states in small superconducting disks for $L = 0$ to 40. Well-defined shell structures were found over the entire vorticity range, and quantitative analysis of their evolution with increasing L allowed us to identify the rules of shell filling and find magic numbers.

Our mesoscopic samples were made from a 150 nm Nb film deposited on a Si substrate using magnetron sputtering [the measured transition temperature $T_c = 9.1$ K and critical field $H_{c2}(0) \approx 1.5$ T were used to estimate magnetic penetration depth $\lambda(0)$ as ≈ 90 nm and coherence length $\xi(0)$ as ≈ 15 nm [18]]. The Bitter decoration technique used in the experiments is described in detail in Ref. [19] and based on *in situ* evaporation of 10–20 nm Fe particles that are attracted to regions of magnetic field created by individual vortices and thus allow their visualization. Figure 1(a) shows a typical vortex structure in the macroscopic film. The uniform but disordered vortex arrangement is a signature of the presence of pinning (see, e.g., [19]), typical for sputtered Nb films. Using e-beam lithography and dry etching, the film was made into large arrays of mesoscopic ''dots''—disks, triangles, and squares of 4 different sizes: $\approx$1, 2, 3, and 5 μm [Fig. 1(b) shows part

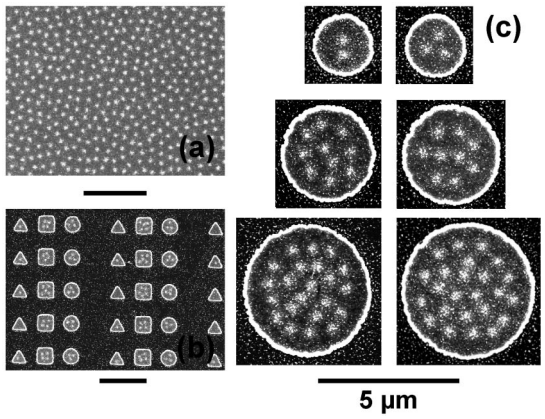

FIG. 1. Scanning electronic microscope (SEM) images of vortex patterns obtained after field cooling to 1.8 K in (a) macroscopic film ($H = 30$ Oe), (b) part of an array containing $\sim$2 μm dots ($H = 40$ Oe), (c) vortex configurations in disks with $d = 2.3$, 3.4, and 5.0 μm obtained in the same experiment at $H = 40$ Oe. Scale bars in all images correspond to 5 μm.

of an array containing ~2 μm dots]. A whole array, containing over 500 dots, was decorated in each of over 20 experiments, allowing us to obtain snapshots of about a hundred vortex configurations in nominally identical samples under identical conditions (field H, temperature T, etc.). It was therefore possible not only to simultaneously visualize vortex configurations in samples of different sizes but also to gain enough statistics for their analysis in terms of stability, sensitivity to shape irregularities, etc. Below, we focus on the results obtained for the disk geometry after field cooling to $T \approx 1.8$ K [20] in homogeneous perpendicular H from 20 to 160 Oe.

Figure 1(c) shows an example of vortex configurations observed in the same experiment on disks of three diameters d. The images illustrate the excellent resolution achieved in our studies, as well as the main features of observed vortex patterns. For $L = 1$ to 5, vortices were found to arrange into simple symmetric structures (at $L = 1$ the vortex sits in the center; $L = 2$ is shown in Fig. 1; $L = 3, 4$, and 5 form a triangle, square, and ring, respectively). As L increases further, vortices start to form concentric shells, e.g., two shells in 3.4 μm disks and three shells in 5 μm disks of Fig. 1(c). Using the standard notation for confined geometries [2–4,12,13], we refer to the states of Fig. 1(c) as (2), (3), (2, 7), (2, 8), (2, 7, 13), and (3, 8, 13). It is clear that, despite the presence of pinning, vortices generally form circular configurations expected for disk geometry; i.e., the effect of confinement dominates over pinning. This was found to be the case for all $L \leq 40$. At larger L, vortices in the center no longer "feel" the presence of the boundary, and pinning is only opposed by vortex-vortex interactions [15]. Accordingly, vortex patterns become increasingly disordered, as expected for collective pinning [21], and eventually (for $L > 100$) reminiscent of that in the macroscopic film.

The observed relationship between L and the magnetic flux $\Phi = H \cdot S$ through the disk area S is shown in Fig. 2. For all L, the flux required to form L vortices is considerably larger than $\Phi_0 L$ (see Fig. 2). This result becomes clearer when plotted as an excess flux $\delta\Phi$ (compared to Φ_0) needed to add one vortex to state $(L - 1)$ [22]. Indeed, a total flux $\sim 3.5\Phi_0$ is required for the formation of the first vortex, $\sim 2.8\Phi_0$ for the addition of the second one, etc. Accordingly, the states with $L < 5$ are stable over appreciable field intervals ΔH (e.g., $L = 1$ in a 2 μm disk is stable over $\Delta H \approx 20$ Oe; $L = 2$ over $\Delta H \approx 10$ Oe). At $L > 10$ the excess flux saturates at $\delta\Phi \approx 0.2\Phi_0$, which can be explained by finite ("edge") demagnetization in the limit of large L [3]. The observed behavior is in agreement with results of numerical analysis [3] (see fits in Fig. 2).

The observed excess flux corresponds to a strong diamagnetic response of our disks, and the agreement with theory indicates further that the observed vortex configurations were close to thermodynamically stable. This might seem somewhat unusual because field cooling is known to result in extra vortices captured inside due to the presence of the edge [1–4,8,16,23]. We clearly do not observe this in our experiments, which is attributed [8,10,23] to the relatively rough edges of our disks, as these allow extra vortices to escape so that vortex configurations approach their low-temperature equilibrium. This allows us to refer to the most frequently observed patterns as stable [24].

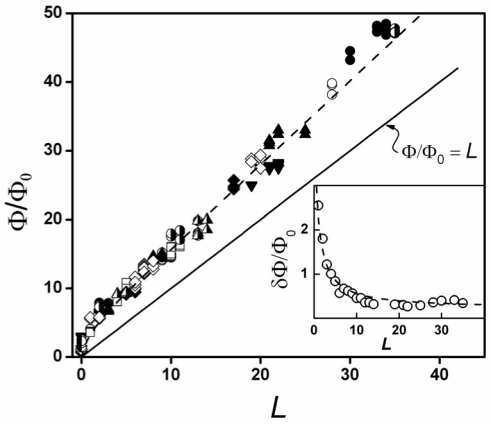

FIG. 2. Vorticity L vs normalized flux through disk area, Φ/Φ_0. Data points show measurements for individual disks rather than a statistical average. Different symbols correspond to different experiments. The inset shows normalized excess flux $\delta\Phi/\Phi_0 = (\Phi - \Phi_0 L)/\Phi_0 L$ (see text). The dashed line shows a fit to the function $\delta\Phi/\Phi_0 = (a + bL)/(1 + cL)$ (see [3]). The corresponding fit for Φ/Φ_0 vs L is shown by the dashed line in the main panel.

For $L \leq 4$ only one vortex configuration was found for each L. For larger L, however, at least two or more configurations were found in any given experiment (i.e., in the same H, under identical conditions). This is demonstrated by the histogram in Fig. 3(a) where, first, two vorticities ($L = 9$ and $L = 10$) and, second, three distinct states for each L were observed in the same experiment for disks of nominally the same d. The two vorticities can be explained by slightly different shapes of individual disks or an extra vortex captured during field cooling as discussed above. However, the observed multiplicity of states for the same L and Φ is unexpected. Indeed, different states were found in the same experiment even for disks with the same area, smooth boundaries, and minimal deviations from the circular shape [see, e.g., images (2, 8) and (3, 7) in Fig. 3(a)]. The only plausible explanation is that we observe not only stable states of L interacting vortices but also their metastable configurations [2–4,6,23]. Indeed, in all experiments one of the configurations for a given L was observed typically twice as frequently than the others [see Fig. 3(a)], indicating that it has a larger interval of stability [3,4]. We therefore identify this configuration as stable and refer to the others as metastable states for a given L. The results of such analysis are summarized in Table I. Most configurations found experimentally agree with numerical simulations [2–4] (states $L = 1$ to 5, $L = 7$, and $L = 8$). However, the predicted state (6) (all 6 vortices in one shell) was found in just 5% of the cases, indicating that it is much less stable than state (1, 5) with

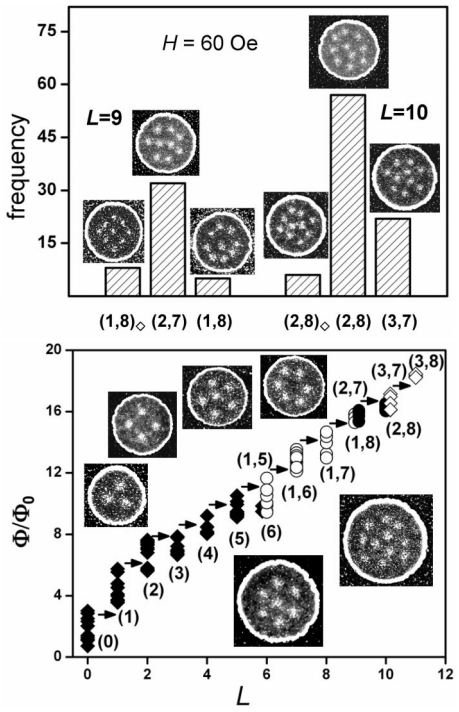

FIG. 3. (a) Histogram of different vortex states observed in the same experiment ($H = 60$ Oe) on disks with $d = 3$ μm. SEM images of the corresponding states are shown as insets. (b) Evolution of vortex states with increasing Φ (arrows are guides to the eye). Different symbols correspond to different shell configurations: ◆, states (L); ○, states $(1, L-1)$; ●, states $(2, L-2)$; ◇, states $(3, L-3)$. SEM images of some of the states are shown as insets: left to right states (3), (4), (1, 5), (6), (1, 6), and (3,8).

a vortex in the center. Similarly, for $L = 9$ the predicted configuration (1, 8) was found in just a few cases, mostly with a square, rather than circular, symmetry [Fig. 3(a)]. The predicted states (1, 9) and (2, 9) were never seen in our experiments. On the other hand, as one can see from Table I that the observed vortex configurations are in better agreement with those predicted for a finite system of charged particles [12] and vortices in liquid helium [13]. The agreement between our observations and predictions for completely different confined systems provides more proof of the common physics governing various systems.

The square-symmetry states $(1, 8)_\diamond$ and $(2, 8)_\diamond$ shown in Fig. 3(a) are notable exceptions from the general rule where, as expected for the disk symmetry, vortex positions fall closely into concentric rings. In state $(1, 8)_\diamond$ the 8 outer vortices sit on the perimeter of a square, rather than on a ring, effectively having the same fourfold symmetry as state (4) shown in Fig. 3(b). This effect is unlikely to be due to pinning of some of the vortices, because state $(1, 8)_\diamond$ was observed in many experiments and, in fact, more frequently than the circular state (1, 8). One possible explanation is that the square-symmetry states might become energetically more favorable because they correspond to a square vortex lattice, which is a known modification of the usual triangular lattice and is found in, e.g., anisotropic superconductors. To check this, calculations of stability for vortex states with square and circular symmetries are required, which are not available at the moment.

In terms of the relationship between L and the total flux, it was not possible to distinguish between different states with the same L, as one can see in Fig. 3(b). For example, the rarely observed state (1, 8) and the stable state (2, 7) are found over the same interval of Φ/Φ_0. At the same time, as Fig. 3(b) demonstrates, we could trace the exact evolution of vortex states as L increased with increasing flux. States with different L are realized over overlapping intervals of Φ and their evolution follows a well-defined pattern. The first 5 vortices are added one by one to form the first shell, the second shell appears at $L = 6$ in the form of one vortex in the center [state (1, 5) in Fig. 3(b)], and this configuration remains stable until $L = 9$ is reached, i.e., the next 3 vortices are added to the outer shell. The inner shell begins to grow at $L = 9$, with the next two states having 2 vortices in the center [(2, 7) and (2, 8) in Fig. 3(a)], the

TABLE I. Comparison of experimentally observed stable (S_{exp}) and metastable (MS_{exp}) states for $1 \leq L \leq 11$ with those found numerically. Only stable (ground) states were calculated in Ref. [12].

L	S_{exp}		S_{theory}		MS_{exp}	MS_{theory}	
1	(1)	(1)[a]	(1)[b]	(1)[c]	⋯	⋯	⋯
2	(2)	(2)[a]	(2)[b]	(2)[c]	⋯	⋯	⋯
3	(3)	(3)[a]	(3)[b]	(3)[c]	⋯	⋯	⋯
4	(4)	(4)[a]	(4)[b]	(4)[c]	⋯	⋯	⋯
5	(5)	(5)[a]	(5)[b]	(5)[c]	(1, 4)	⋯	(1, 4)[b]
6	(1, 5)	(6)[a]	(1, 5)[b]	(1, 5)[c]	(6)	(1, 5)[a]	(6)[b]
7	(1, 6)	(1, 6)[a]	(1, 6)[b]	(1, 6)[c]	⋯	(7)[a]	(7)[b]
8	(1, 7)	(1, 7)[a]	(1, 7)[b]	(1, 7)[c]	⋯	(8)[a]	⋯
9	(2, 7)	(1, 8)[a]	(1, 8)[b]	(2, 7)[c]	(1, 8); $(1, 8)_\diamond$	⋯	(2, 7); (3, 6)[b]
10	(2, 8)	(1, 9)[a]	(2, 8)[b]	(2, 8)[c]	(3, 7); $(2, 8)_\diamond$	(2, 8)[a]	(1, 9)[b]
11	(3, 8)	(2, 9)[a]	(3, 8)[b]	(3, 8)[c]	(4, 7)	(1, 10); (3, 8)[a]	(2, 9)[b]

[a]Results of Ref. [4] for superconducting vortices.
[b]Vortices in He [13].
[c]Charged particles [12].

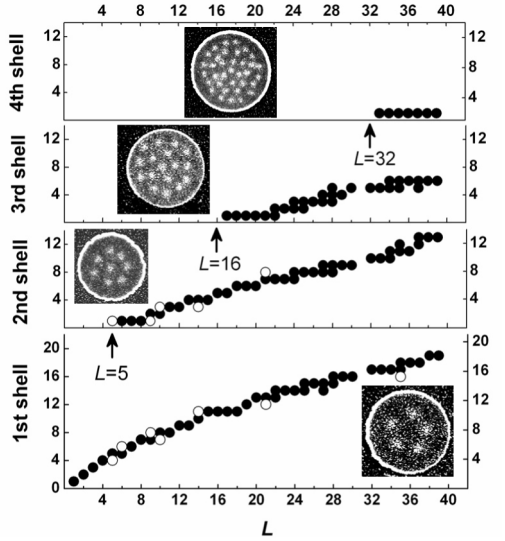

FIG. 4. Number of vortices populating different shells as a function of L. Two or more different states were found for some vorticities (see text), e.g., (1, 7, 14) and (2, 7, 13) for $L = 22$, (1, 5, 12, 17), (1, 5, 11, 18), (1, 6, 11, 17), and (1, 6, 12, 16) for $L = 35$, etc. Open circles show numbers of vortices in a shell corresponding to the configurations that we could clearly identify as metastable. Arrows indicate magic numbers, i.e., L corresponding to closed shell configurations, just before the appearance of the 2nd, 3rd, and 4th shell. The first magic number, $L = 5$, corresponds to the stable state (5) rather than the metastable state (1, 4). Insets: SEM images of vortex states with different numbers of shells: 1-shell state (5) [$L = 5$]; 2-shell state (1, 7) [$L = 8$]; 3-shell state (1, 5, 11) [$L = 17$]; 4-shell state (1, 5, 11, 18) [$L = 35$].

following two states having 3 vortices in the center [(3, 7) in Fig. 3(a) and (3, 8) in Fig. 3(b)], and so on.

The process of shell filling for all L up to 40 is summarized in Fig. 4. For $L = 12$ to 16, vortices are added intermittently to either the outer or the inner shell. At $L = 17$ the third shell appears, again in the form of one vortex in the center. The next 3 vortices are added to the outermost shell, after which all three shells grow intermittently until $L = 32$. The fourth shell appears at $L = 33$ in the form of one vortex in the center, and a process identical to the evolution of the previous shells is repeated again. Note that vortex patterns with one vortex in the center are particularly stable, as they are observed for several consecutive L. Indeed, this seems to be a property of vortex configurations closest to the triangular lattice, i.e., of states (1, 6), (1, 7), (1, 6, 12), etc. [13]. The stability of states (1, 5), (1, 6), and (1, 7) over larger intervals of H is also evident from Fig. 3(b). Furthermore, once a new shell appears, the vortex configuration never reverses to the previous number of shells and there is a clear tendency that the next few vortices are added to the next but one shell. Thus we can unambiguously identify vorticities corresponding to one, two, and three ''complete'' shells. We emphasize that L values corresponding to the appearance of new shells are very robust (reproduced in many experiments for different H and d) and therefore can be viewed as magic numbers. For our system these are $L = 5$, 16, and 32 as indicated by arrows in Fig. 4.

The above pattern of shell filling for vortices is somewhat reminiscent of the formation of shells in atoms and nuclei. Unfortunately, at the moment there is no theory that would explain the background physics mechanism responsible for populating each vortex shell, e.g., similar to Hund's rules. It would be interesting to identify such rules qualitatively, in addition to the current understanding [2–4,15] that the appearance of each new shell is somehow dictated by achieving the lowest energy.

*To whom correspondence should be addressed

[1] V. A. Schweigert, F. M. Peeters, and P. Singha Deo, Phys. Rev. Lett. **81**, 2783 (1998).
[2] A. I. Buzdin and J. P. Brison, Phys. Lett. A **196**, 267 (1994); J. J. Palacios, Phys. Rev. B **58**, R5948 (1998).
[3] B. J. Baelus and F. M. Peeters, Phys. Rev. B **65**, 104515 (2002).
[4] B. J. Baelus, L. R. E. Cabral, and F. M. Peeters, Phys. Rev. B **69**, 064506 (2004).
[5] H. J. Fink and A. G. Presson, Phys. Rev. **151**, 219 (1966); V. V. Moshchalkov, X. G. Qiu, and V. Bruyndoncx, Phys. Rev. B **55**, 11 793 (1997).
[6] V. A. Schweigert and F. M. Peeters, Physica (Amsterdam) **332C**, 266 (2000); **332C**, 426 (2000).
[7] L. F. Chibotaru *et al.*, Nature (London) **408**, 833 (2000).
[8] A. K. Geim *et al.*, Nature (London) **396**, 144 (1998).
[9] A. Kanda *et al.*, Phys. Rev. Lett. **93**, 257002 (2004).
[10] A. K. Geim *et al.*, Nature (London) **407**, 55 (2000).
[11] A. Bezryadin *et al.*, Phys. Rev. B **53**, 8553 (1996).
[12] V. M. Bedanov and F. M. Peeters, Phys. Rev. B **49**, 2667 (1994).
[13] L. J. Campbell and R. M. Ziff, Phys. Rev. B **20**, 1886 (1979).
[14] A. L. Fetter and A. A. Svidzinsky, J. Phys. Condens. Matter **13**, R135 (2001).
[15] L. R. E. Cabral, B. J. Baelus, and F. M. Peeters, Phys. Rev. B **70**, 144523 (2004).
[16] A. K. Geim *et al.*, Nature (London) **390**, 259 (1997); Phys. Rev. Lett. **85**, 1528 (2000).
[17] T. Nishio *et al.*, Physica (Amsterdam) **412C–414C**, 379 (2004).
[18] A. F. Mayadas, R. B. Laibowitz, and J. J. Cuomo, J. Appl. Phys. **43**, 1287 (1972).
[19] I. V. Grigorieva, Supercond. Sci. Technol. **7**, 161 (1994).
[20] Thermal evaporation of Fe particles usually leads to a temporary increase in temperature of decorated samples, but the increase never exceeded 2 K in our experiments, leaving the Nb dots in the low-temperature limit $T < 0.5T_c$.
[21] G. Blatter *et al.*, Rev. Mod. Phys. **66**, 1125 (1994).
[22] $\delta\Phi$ was calculated from the minimum Φ for a given L.
[23] V. A. Schweigert and F. M. Peeters, Phys. Rev. B **57**, 13 817 (1998).
[24] Strictly speaking, we study stable and metastable configurations of L vortices rather than a thermodynamically stable state of a given superconductor.